Ground-state configurations and unresolved transition arrays in extreme ultraviolet spectra of lanthanide ions

D. Kilbane[*] and G. O'Sullivan

School of Physics, University College Dublin, Belfield, Dublin 4, Ireland

Theoretical ground-state configurations of lanthanide ions calculated with the Cowan suite of codes are presented. Theoretical $4d$-$4f$ and $4p$-$4d$ spectra of Pd-like to Rb-like lanthanide ions calculated using the relativistic flexible atomic code are also shown. The effects of configuration interaction are investigated, and the results compare favorably with experiments in which, for increasing nuclear charge, strong emission peaks are observed to move toward shorter wavelength. The application of these strong emitters as extreme ultraviolet radiation sources, a topic of emerging interest, is discussed.

I. INTRODUCTION

In 2003, Biemont and Quinet produced a comprehensive study of the structure and spectra of lanthanide atoms and ions [1]. They reviewed known experimental and theoretical spectra, transition probabilities, radiative lifetimes, hyperfine structures, and isotope shifts. Currently, ground-state configurations of the lanthanides are known experimentally for ion stages up to the third and in some cases the fourth stage [2]. As noted in [1], systematic analysis of spectra in higher ion stages of lanthanum and cerium have been performed: La VII [3], La VIII [4], La IX [5–8], La X [9], La XI [10,11], La XIII [12], Ce III [13], Ce V [14], Ce VI [15], Ce IX [16], Ce X [17], and Ce XIV [10–12]. More recently, progress has been made in analyzing Cd-like ion spectra from Xe VII–Eu XVI [5,18,19] and Pd-like ion spectra [20].

In 1981, O'Sullivan and Carroll performed the first systematic recording of $4d$-$4f$ emission in cesium through lutetium using the laser-produced plasma (LPP) technique [21]. The spectra displayed relatively narrow regions of resonancelike emission which became more complex and moved to shorter wavelength with increasing nuclear charge, Z. They attributed these emissions in a given element to $4d$-$4f$ transitions overlapping from several adjacent ions. A complementary work by the same authors [22] predicted from experimental results the ground-state configurations of ions I through XVI for $Z = 57$–74. This aided the interpretation of $4d$-$4f$ emission in the lanthanides and linked the complexity in the spectra to $4f$ electron occupancy in the ground state.

Since then, there has been much research done to understand the origin of these complicated spectra. Mandelbaum *et al.* [23] used the unresolved transition array (UTA) model developed by Bauche-Arnoult, Bauche, and Klapisch [24–27], and they carried out *ab initio* calculations on La to Eu using the relativistic RELAC code [28] to account for configuration interaction (CI). They concluded that interactions between the $4p^6 4d^{N-1} 4f$ and $4p^5 4d^{N+1}$ configurations are responsible for narrowing the transition arrays and their superposition in adjacent ion stages. This theory was supported by the recording of absolutely calibrated soft-x-ray spectra from laser plasmas

of various materials with atomic numbers ranging from 57 to 82 [29].

The motivation for this work arose from a number of factors: (i) It is a natural theoretical follow-up to the earlier experimental work of Carroll and O'Sullivan [22]; (ii) the techniques used for the analysis of the experimental spectra of gadolinium and terbium [30] can be applied to similar lanthanide ions; (iii) we wanted to search for a successor at shorter wavelengths to tin, xenon, and lithium plasmas as a source for extreme ultraviolet (EUV) lithography; (iv) we wanted to search for an x-ray ultraviolet (XUV) and soft-x-ray source for metrology to be used in microscopes for biological sampling; and finally (v) we wanted to provide a comprehensive overview of trends in theoretical atomic structure and spectra along the lanthanide series. In Sec. II, we present the results of calculated ground-state configurations of Ag-like to Ho-like lanthanide ions. In Sec. III, we present 180 theoretical $4d$-$4f$ and $4p$-$4d$ UTA spectra for ions with configurations $4p^6 4d^N$-$4p^6 4d^{N-1} 4f$ and $4p^6 4d^N$-$4p^5 4d^{N+1}$, $N = 1, \ldots, 10$. Also in this section, we discuss the effects of CI and overall trends in the position and intensity of UTA peaks from La to Lu. Finally, in Sec. IV we conclude with a summary of this study of lanthanide ions.

II. GROUND-STATE CONFIGURATIONS OF LANTHANIDE IONS

As in [30,31], *ab initio* calculations were performed using the Hartree-Fock approximation with the relativistic and correlation corrections mode of the Cowan suite of atomic codes [32] for the lanthanide ions. It is well known that the $4f$ binding energy increases more rapidly with increasing ionization than that of either $5p$ or $5s$, which leads to significant reordering of configuration energies. All configurations considered from Ag-like to Ho-like ions are presented in Table I. In this table, $M + N + K = 6$ means that configuration average energies of $5s^2 5p^4$, $5s^2 5p^3 4f$, $5s^2 5p^2 4f^2$, $5s^2 5p 4f^3$, $5s^2 4f^4$, $5s 5p^5$, $5s 5p^4 4f$, $5s 5p^3 4f^2$, $5s 5p^2 4f^3$, $5s 5p 4f^4$, $5s 4f^5$, $5p^6$, $5p^5 4f$, $5p^4 4f^2$, $5p^3 4f^3$, $5p^2 4f^4$, $5p 4f^5$, and $4f^6$ were calculated. The ground-state configuration was taken as the one with the lowest calculated average energy [33,34], and the results are illustrated comprehensively in Fig. 1 and Table II.

———————
[*]Deirdre.Kilbane@ucd.ie

TABLE I. Configurations of the type $5s^M 5p^K 4f^N$ included in the calculation of configuration average energies E_{av} to determine the ground-state configuration.

Sequence	$M + K + N$	Sequence	$M + K + N$
Ag-like	1	Ce-like	12
Cd-like	2	Pr-like	13
In-like	3	Nd-like	14
Sn-like	4	Pm-like	15
Sb-like	5	Sm-like	16
Te-like	6	Eu-like	17
I-like	7	Gd-like	18
Xe-like	8	Tb-like	19
Cs-like	9	Dy-like	20
La-like	11	Ho-like	21

As noted by Carroll and O'Sullivan [22], knowing the behavior of the $4f$ electron is crucial for an understanding of the ground-state configurations of the lanthanides in their various stages of ionization. The ground states for the neutrals and the first three ion stages are known experimentally [2] and are presented in Table I of [22]. In order to establish a trend in the ground-state configurations, we look at the Xe-like sequence. Figure 1(c) highlights the position where a crossover from $5p$ to $4f$ occupancy in the ground-state configuration occurs. In the earlier work [22], it was proposed (based on experimental evidence) that the ground-state configuration was $5s^2 5p^6$ from La IV–Pr VI, which is consistent with our current calculations. (Discrepancies between the current study and previous work [22] are highlighted in bold in Table II.) Following this, it was expected that due to $4f$-wave-function collapse, from which the $4f$ electron becomes more tightly bound than the $5p$ electron, the ground-state configuration would be $5s^2 4f^6$ for Nd VII–Ho XIV, as presented in Table I of [22]. Our calculations disagree for Nd VII–Eu X, where the ground-state configuration is found to be $5s^2 5p^6$ for Nd VII, $5s^2 5p^5 4f$ for Pm VIII, $5s^2 5p^3 4f^3$ for Sm IX, $5s^2 5p^2 4f^4$
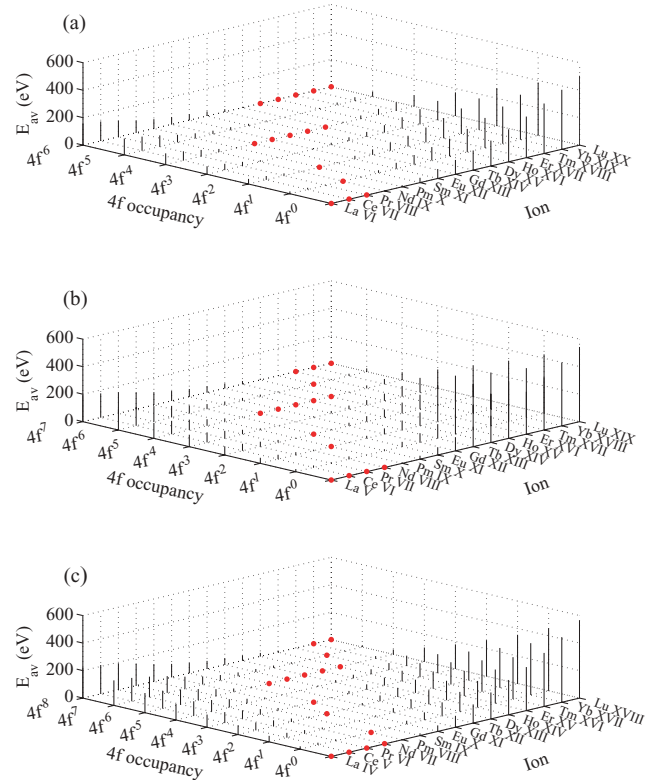

FIG. 1. (Color online) Configuration average energies E_{av} of the Te-like to Xe-like ions: (a) Te-like, (b) I-like, and (c) Xe-like ions [red (dark gray) dots denote ground configuration].

for Eu X, and $5s^2 4f^6$ for Gd XI. This would indicate that the best description is contraction rather than collapse, and there is considerable interaction between the $5p$ and $4f$ orbitals until Gd XI. It was also predicted that the ground-state configuration for Er XV and Yb XVI would be $4d^{10} 4f^8$. We calculated $5s^2 4d^{10} 4f^6$ for Er XV and $5s 4d^{10} 4f^7$ for Yb XVI, which again indicates an interplay of the $5s$ and $4f$ orbitals at the

TABLE II. Ground-state configurations of ions in stages V–XVII for elements lanthanum through hafnium. Discrepancies between the current table and Table I of [22] are highlighted in bold.

	V	VI	VII	VIII	IX	X	XI	XII	XIII	XIV	XV	XVI	XVII
La	$5s^2 5p^5$	$5s^2 5p^4$	$5s^2 5p^3$	$5s^2 5p^2$	$5s^2 5p$	$5s^2$	$5s$	$4d^{10}$	$4d^9$	$4d^8$	$4d^7$	$4d^6$	$4d^5$
Ce	$5s^2 5p^6$	$5s^2 5p^5$	$\mathbf{5s^2 5p^4}$	$\mathbf{5s^2 5p^3}$	$\mathbf{5s^2 5p^2}$	$\mathbf{5s^2 5p}$	$5s^2$	$5s$	$4d^{10}$	$4d^9$	$4d^8$	$4d^7$	$4d^6$
Pr	$5p^6 4f$	$5s^2 5p^6$	$\mathbf{5s^2 5p^5}$	$\mathbf{5s^2 5p^4}$	$\mathbf{5s^2 5p^3}$	$\mathbf{5s^2 5p^2}$	$5s^2 4f$	$5s^2$	$5s$	$4d^{10}$	$4d^9$	$4d^8$	$4d^7$
Nd	$5p^6 4f^2$	$5p^6 4f$	$\mathbf{5s^2 5p^6}$	$\mathbf{5s^2 5p^5}$	$\mathbf{5p^3 4f}$	$\mathbf{5p^2 4f}$	$5s^2 4f^2$	$5s^2 4f$	$5s^2$	$5s$	$4d^{10}$	$4d^9$	$4d^8$
Pm	$5p^6 4f^3$	$5p^6 4f^2$	$\mathbf{5p^6 4f}$	$\mathbf{5p^5 4f}$	$\mathbf{5p^3 4f^2}$	$\mathbf{5p^2 4f^2}$	$5s^2 4f^3$	$5s^2 4f^2$	$5s^2 4f$	$5s^2$	$4f$	$4d^{10}$	$4d^9$
Sm	$5p^6 4f^4$	$5p^6 4f^3$	$\mathbf{5p^6 4f^2}$	$\mathbf{5p^5 4f^2}$	$\mathbf{5p^3 4f^3}$	$\mathbf{5p^2 4f^3}$	$5s^2 4f^4$	$5s^2 4f^3$	$5s^2 4f^2$	$5s^2 4f$	$\mathbf{5s4f}$	$4f$	$4d^{10}$
Eu	$5p^6 4f^5$	$5p^6 4f^4$	$\mathbf{5p^6 4f^3}$	$\mathbf{5p^5 4f^3}$	$\mathbf{5p^3 4f^4}$	$\mathbf{5p^2 4f^4}$	$5s^2 4f^5$	$5s^2 4f^4$	$5s^2 4f^3$	$5s^2 4f^2$	$\mathbf{5s4f^2}$	$4f^2$	$4f$
Gd	$5p^6 4f^6$	$5p^6 4f^5$	$\mathbf{5p^6 4f^4}$	$\mathbf{5p^5 4f^4}$	$\mathbf{5p^4 4f^4}$	$\mathbf{5p^2 4f^5}$	$5s^2 4f^6$	$5s^2 4f^5$	$5s^2 4f^4$	$5s^2 4f^3$	$\mathbf{5s4f^3}$	$4f^3$	$4f^2$
Tb	$5p^6 4f^7$	$5p^6 4f^6$	$\mathbf{5p^6 4f^5}$	$\mathbf{5p^5 4f^5}$	$\mathbf{5p^4 4f^5}$	$\mathbf{5p^2 4f^6}$	$5s^2 4f^7$	$5s^2 4f^6$	$5s^2 4f^5$	$5s^2 4f^4$	$\mathbf{5s4f^4}$	$4f^4$	$4f^3$
Dy	$5p^6 4f^8$	$5p^6 4f^7$	$\mathbf{5p^6 4f^6}$	$\mathbf{5p^5 4f^6}$	$\mathbf{5p^4 4f^6}$	$\mathbf{5p^2 4f^7}$	$\mathbf{5p4f^7}$	$5s^2 4f^7$	$5s^2 4f^6$	$5s^2 4f^5$	$\mathbf{5s^2 4f^4}$	$4f^5$	$4f^4$
Ho	$5p^6 4f^9$	$5p^6 4f^8$	$\mathbf{5p^6 4f^7}$	$\mathbf{5p^5 4f^7}$	$\mathbf{5p^4 4f^7}$	$\mathbf{5p^2 4f^8}$	$\mathbf{5p4f^8}$	$5s^2 4f^8$	$5s^2 4f^7$	$5s^2 4f^6$	$\mathbf{5s^2 4f^5}$	$4f^6$	$4f^5$
Er	$5p^6 4f^{10}$	$5p^6 4f^9$	$\mathbf{5p^6 4f^8}$	$\mathbf{5p^5 4f^8}$	$\mathbf{5p^4 4f^8}$	$\mathbf{5p^2 4f^9}$	$\mathbf{5p4f^9}$	$5s^2 4f^9$	$5s^2 4f^8$	$5s^2 4f^7$	$\mathbf{5s^2 4f^6}$	$\mathbf{5s4f^6}$	$4f^6$
Tm	$5p^6 4f^{11}$	$5p^6 4f^{10}$	$\mathbf{5p^6 4f^9}$	$\mathbf{5p^6 4f^8}$	$\mathbf{5p^4 4f^9}$	$\mathbf{5p^2 4f^{10}}$	$\mathbf{5p4f^{10}}$	$5s^2 4f^{10}$	$5s^2 4f^9$	$5s^2 4f^8$	$\mathbf{5s^2 4f^7}$	$\mathbf{5s4f^7}$	$4f^7$
Yb	$5p^6 4f^{12}$	$5p^6 4f^{11}$	$\mathbf{5p^6 4f^{10}}$	$\mathbf{5p^6 4f^9}$	$\mathbf{5p^4 4f^{10}}$	$\mathbf{5p^3 4f^{10}}$	$\mathbf{5p4f^{11}}$	$5s^2 4f^{11}$	$5s^2 4f^{10}$	$5s^2 4f^9$	$\mathbf{5s^2 4f^8}$	$\mathbf{5s4f^8}$	$4f^8$
Lu	$5p^6 4f^{13}$	$5p^6 4f^{12}$	$\mathbf{5p^6 4f^{11}}$	$\mathbf{5p^6 4f^{10}}$	$\mathbf{5p^4 4f^{11}}$	$\mathbf{5p^3 4f^{11}}$	$\mathbf{5p4f^{12}}$	$5s^2 4f^{12}$	$5s^2 4f^{11}$	$5s^2 4f^{10}$	$\mathbf{5s^2 4f^9}$	$\mathbf{5s4f^9}$	$4f^9$

fourteenth ion stage, in agreement with [22]. In [34,35] the same sequence was calculated in a noninteracting regime using the Froese-Fischer [36] multiconfiguration Hartree-Fock (MCHF) code. The results presented in Table I of [35] differ considerably in the order of filling of $5p$ versus $4f$ and $5s$ electron occupancy. We now consider the isoionic sequence of ions ionized six times. In [22], it was proposed that once the $4f$ crossing has occurred at Pr VII, the $4f$ shell will continue to fill until Er VII is reached with $5s^24f^{14}$, past which the ground-state configuration would be of the type $5s^24f^{14}5p^l$. We find the order to be $5s^25p^3$ in La VII followed by a successive filling of the $5p$ subshell until $5s^25p^6$ is reached in Nd VII and successive filling of the $4f$ subshell from $5s^25p^64f$ in Pm VII to $5s^25p^64f^{11}$ in Lu VII.

Carroll and O'Sullivan concluded that the $5p$-$4f$ crossing occurs between the fifth and sixth ion stages (corresponding to the VI and VII spectra, respectively) from praseodymium to hafnium with some uncertainty as to its exact location. Based on our current calculations, we predict a similar phenomenon but with a more gradual emptying of the $5p$ subshell, followed by emptying of the $4f$ subshell, for example,

from Pr VII to Pr XI. This confirms the point made in [22] that near the location where $5p$-$4f$ crossing occurs, the lowest configurations may contain both $4f$ and $5p$ electrons, the $5p$ subshell being only partially depopulated. As previously stated, this method of determining ground-state configurations is based on configuration-average energies (E_{av}). In many cases, E_{av} values for different configurations lie very close to the ground-state configuration. For example, for Nd IX, $5s^25p^4$ lies just 0.707 eV above $5s^25p^34f$. Also, there is a very large spread in energy levels for some of these low-lying configurations. For example, for Gd VIII, $5s^25p^54f^4$ spans ≈ 33 eV. Therefore, the E_{av} of one configuration could lie below the E_{av} of another configuration but above the lowest energy level of the latter configuration. In such a case, the former configuration could no longer be considered as the ground-state configuration. The origin of the exact ground-state term is uncertain and is best described as $(5s5p4f)^q$, where q is the total number of electrons shared among $5s$, $5p$, and $4f$ orbitals [35]. However, in the absence of experimentally determined energy levels, and in the presence of configuration mixing, which makes state labeling somewhat ambiguous, the current approach based on E_{av} values is deemed acceptable.
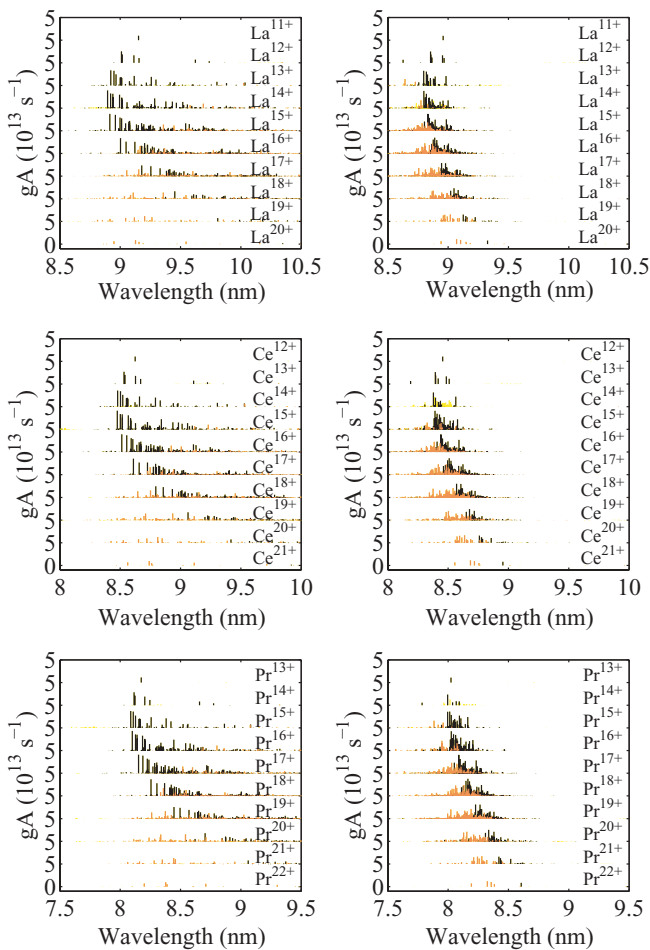

FIG. 2. (Color online) Pd-like through Rb-like spectra of lanthanum, cerium, and praseodymium computed with the FAC, excluding CI (left) and including CI (right). Black denotes $4d$-$4f$ transitions, orange (gray) denotes $4p$-$4d$ transitions, and yellow (light gray) denotes all transitions.
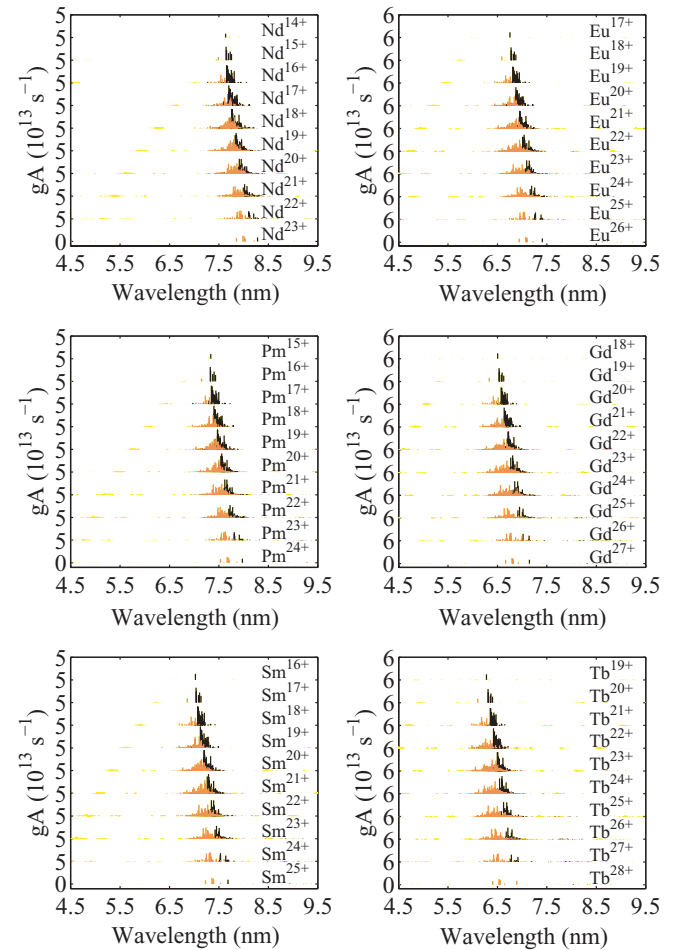

FIG. 3. (Color online) Pd-like through Rb-like spectra of neodymium through terbium computed with the FAC including CI. Black denotes $4d$-$4f$ transitions, orange (gray) denotes $4p$-$4d$ transitions, and yellow (light gray) denotes all transitions.

III. UNRESOLVED TRANSITION ARRAYS OF LANTHANIDE IONS

In the lanthanides, the strongest lines occurring in the EUV result from $4d$-$4f$ and $4p$-$4d$ transitions in ion stages with open $4d$ subshells. Since experimental information is largely lacking for these ions, it is currently not possible to estimate the necessary scaling factors used in the Cowan code for each ion stage of the different elements considered here. Therefore, for consistency we decided on an *ab initio* approach, and calculations were performed with the flexible atomic code (FAC) [37]. This uses a fully relativistic approach based on the Dirac equation, thus allowing its application to ions with large values of nuclear charge. The following basis set was used: $4p^6 4d^N$, $4p^6 4d^{N-1} nl$, and $4p^5 4d^{N+1}$, where $n \leqslant 8$, $l \leqslant 3$, and $1 \leqslant N \leqslant 10$. In a recent study [31], we found that for a range of 24 ions, namely, Gd^{16+}–Gd^{27+} and Tb^{17+}–Tb^{28+}, the FAC spectra were always positioned at a slightly shorter wavelength than the experimental and/or the Cowan spectra. Hence a wavelength correction was subsequently applied to the FAC spectrum calculated for each ion. The largest shift necessary was $\leqslant 0.2$ nm, which gives an estimate of the accuracy of the FAC results. For this reason, we employ the FAC in this work, and all spectra presented in Figs. 2–4 are left unshifted due to a lack of detailed experimental data for comparison.

The effect of CI for Pd-like to Rb-like ions in La to Pr is presented in Fig. 2 (non-CI on the left and CI on the right). CI leads to a narrowing of the peak for all ions considered, especially at the beginning of the lanthanide series. A comparison of the study of Mandelbaum *et al.* [23] and the present spectra shows good agreement among Rh-like, Ru-like, Sr-like, and Rb-like praseodymium. The $4d$-$4f$ and $4p$-$4d$ subsets of the full CI UTA were extracted and are also shown in Figs. 2–4 in black and orange (gray), respectively [all other non-$(n = 4)$-$(n = 4)$ transitions appear in yellow (light gray)]. The $4d$-$4f$ and $4p$-$4d$ UTAs are seen to overlap considerably in the early lanthanides. However, within a given element, for example, Tb^{19+}–Tb^{28+}, both the $4d$-$4f$ and the $4p$-$4d$ UTAs shift to longer wavelength, with the $4d$-$4f$ shift being more prominent. This effect is observed across the lanthanide series except for certain elements toward the end. For example, for Yb and Lu, particularly in higher ion stages, these UTAs are seen to be separated considerably. This effect will be investigated further in a future work on post-lanthanide
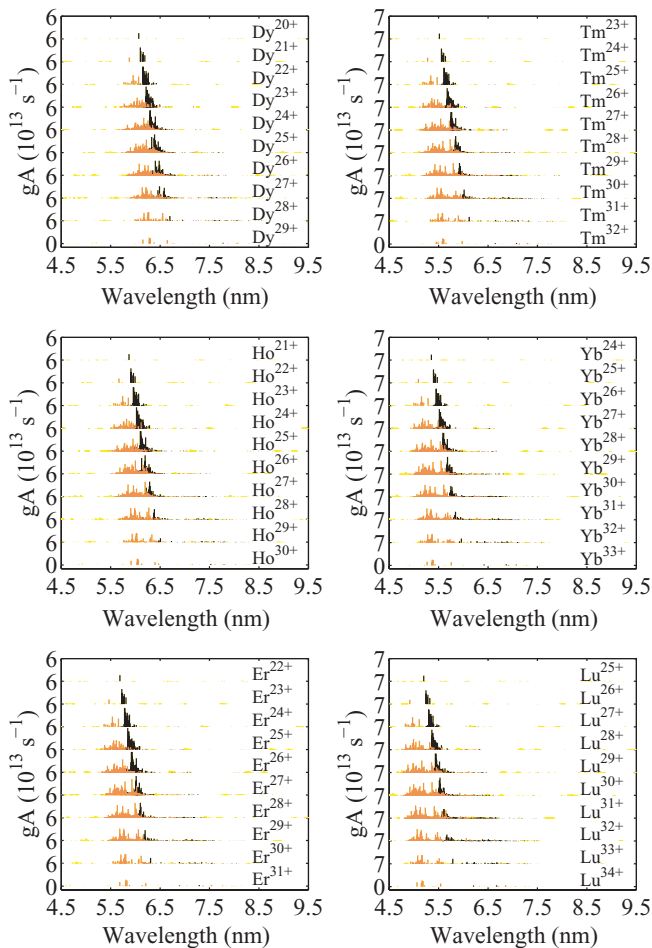

FIG. 4. (Color online) Pd-like through Rb-like spectra of dysprosium through lutetium computed with the FAC including CI. Black denotes $4d$-$4f$ transitions, orange (gray) denotes $4p$-$4d$ transitions, and yellow (light gray) denotes all transitions.
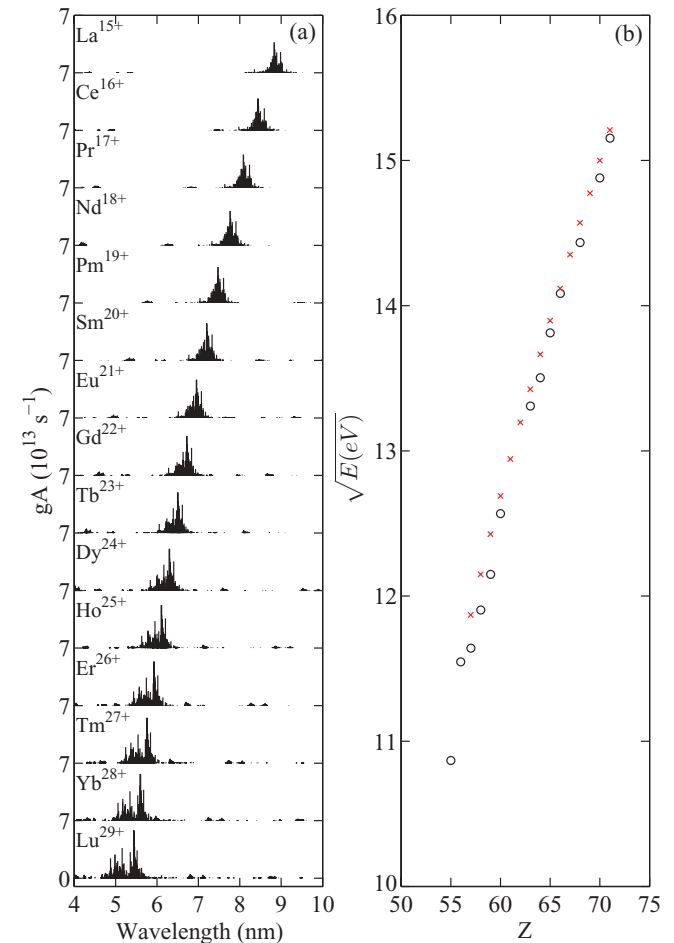

FIG. 5. (Color online) (a) Maximum peak emission from $4d$-$4f$ and $4p$-$4d$ UTAs (including CI) in the lanthanide series. (b) Dependence of UTA transition energies on atomic number Z. Black open circles denote $4d$-$4f$ [21]; red (dark gray) crosses show results from the current work.

elements. However, as these shifts are only minor, the net result is that the position of the peak emission [highest weighted transition probability (gA) values] for a given lanthanide element is seen to remain relatively unchanged as observed for Pr in [23]. In this work, a very small variation of the mean wavelength $\bar{\lambda}$ as a function of the ionization state was reported. For example, for Pr XV–Pr XXIII, $\bar{\lambda}$ varies only from 80.7 to 83.8 Å. This compares favorably with our current calculations, where the wavelength at which maximum peak emission occurs is found to vary only from 80.24 to 83.25 Å for the same ions.

These results are summarized succinctly in Fig. 5. Figure 5(a) shows the ion stage responsible for peak emission in this wavelength range for each lanthanide element. As expected with increasing Z, peak emission moves to shorter wavelength. Note that this peak emission remains comparably large in all elements, and, as previously stated, it remains relatively centered for all ion stages considered. Such a centering of the peak leads us to believe that strong emission can be achieved over a wide range of plasma conditions should any of these elements be considered as an EUV source in the future. Figure 5(b) shows the dependence of $\sqrt{E}$ on nuclear charge, where E is the energy of the point of maximum intensity. Good agreement is observed between the experimental results of [21] and our current calculations, and indeed can be linked to the aforementioned shift between *ab initio* and experimental spectra. It should be noted that the shift decreases with increasing ion stage, a fact that can be traced to the behavior of the $4f$ wave function and its gradual contraction. In lower ion stages, the mean radius of the $4f$ wave function is calculated to be too low, leading to the overestimate of the Slater-Condon parameters, in particular the $G^1(4d,4f)$ integral. This is corrected for by scaling in the Cowan code. As intended by Cowan, the largest adjustment to the scaling factors is required for low ion stages, and the *ab initio* values are approached at high ionization stages.

IV. CONCLUSION

Theoretical ground-state configurations of lanthanide ions calculated with the Cowan suite of codes were presented and discussed in relation to previous experimental and theoretical results. Discrepancies can be attributed to interactions between $5s$, $5p$, and $4f$ orbitals resulting in ambiguities in the assignment of ground-state configurations. These are best described as $(5s5p4f)^q$, where q is the total number of electrons. A total of 180 theoretical $4d$-$4f$ and $4p$-$4d$ UTA spectra for Pd-like to Rb-like ions were calculated using the relativistic FAC. The effects of configuration interaction were investigated, and the results compare favorably with experiments where, for increasing nuclear charge, strong emission peaks are observed to move toward shorter wavelength. The intensity of the maximum emission peak remains comparable for all lanthanide ions and centered for ions within a given element. For these reasons, it is proposed that these strong emitters could be used as EUV, XUV, or soft-x-ray sources in the future. Already, for example, the availability of mirrors with a peak reflectivity of $\approx$40% at 6.7 nm has led to proposals to use gadolinium and terbium emission as potential sources since their peak emission occurs at this wavelength. The proposed application is for lithography beyond 13.5 nm. As more mirrors become available, the other UTA identified here may find applications in this and other fields.

[1] E. Biémont and P. Quinet, Phys. Scr., T **105**, 38 (2003).

[2] W. C. Martin, R. Zalubas, and L. Hagan, *Atomic Energy Levels—The Rare Earth Elements* [Natl. Stand. Ref. Data Ser., Natl. Bur. Stand. **60** (1978)].

[3] R. R. Gayasov, Y. N. Joshi, and A. Tauheed, Phys. Scr. **57**, 565 (1998).

[4] R. Gayasov and Y. N. Joshi, Phys. Scr. **58**, 441 (1998).

[5] V. Kaufman and J. Sugar, J. Opt. Soc. Am. B **4**, 1924 (1987).

[6] S. S. Churilov and Y. N. Joshi, Phys. Scr. **64**, 34 (2001).

[7] R. Gayasov and Y. N. Joshi, J. Opt. Soc. Am. B **15**, 2614 (1998).

[8] A. Tauheed, Y. N. Joshi, and E. H. Pinnington, J. Phys. B **25**, L561 (1992).

[9] R. Gayasov, Y. N. Joshi, and A. N. Ryabtsev, Phys. Scr. **59**, 419 (1999).

[10] R. Gayasov and Y. N. Joshi, J. Phys. B **31**, L705 (1998).

[11] V. Kaufman and J. Sugar, Phys. Scr. **24**, 738 (1981).

[12] R. Gayasov and Y. N. Joshi, Phys. Scr. **60**, 225 (1999).

[13] J.-F. Wyart and P. Palmeri, Phys. Scr. **58**, 368 (1998).

[14] A. Redfors and J. Reader, Phys. Rev. A **43**, 2367 (1991).

[15] S. S. Churilov and Y. N. Joshi, J. Opt. Soc. Am. B **17**, 2081 (2000).

[16] Y. N. Joshi, A. N. Ryabtsev, and S. S. Churilov, J. Opt. Soc. Am. **18**, 1935 (2001).

[17] Y. N. Joshi, A. N. Ryabtsev, and S. S. Churilov, Phys. Scr. **64**, 326 (2001).

[18] S. S. Churilov and Y. N. Joshi, Phys. Scr. **68**, 128 (2003).

[19] S. S. Churilov, Y. N. Joshi, and A. N. Ryabtsev, Phys. Scr. **71**, 43 (2005).

[20] S. S. Churilov, A. N. Ryabtsev, J.-F. Wyart, W.-U. L. Tchang-Brillet, and Y. N. Joshi, Phys. Scr. **71**, 589 (2005).

[21] G. O'Sullivan and P. K. Carroll, J. Opt. Soc. Am. **71**, 227 (1981).

[22] P. K. Carroll and G. O'Sullivan, Phys. Rev. A **25**, 275 (1982).

[23] P. Mandelbaum, M. Finkenthal, J. L. Schwob, and M. Klapisch, Phys. Rev. A **35**, 5051 (1987).

[24] C. Bauche-Arnoult, J. Bauche, and M. Klapisch, Phys. Rev. A **20**, 2424 (1979).

[25] C. Bauche-Arnoult, J. Bauche, and M. Klapisch, Phys. Rev. A **25**, 2641 (1982).

[26] J. Bauche, C. Bauche-Arnoult, E. Luc-Koenig, J.-F. Wyart, and M. Klapisch, Phys. Rev. A **28**, 829 (1983).

[27] C. Bauche-Arnoult, J. Bauche, and M. Klapisch, Phys. Rev. A **31**, 2248 (1985).

[28] M. Klapisch, J. L. Schwob, B. S. Fraenkel, and J. Oreg, J. Opt. Soc. Am. **67**, 148 (1977).

[29] G. M. Zeng, H. Daido, T. Nishikawa, H. Takabe, S. Nakayama, H. Aritome, K. Murai, Y. Kato, M. Nakatsuka, and S. Nakai, J. Appl. Phys. **75**, 1923 (1994).

[30] T. Otsuka, D. Kilbane, J. White, T. Higashiguchi, N. Yugami, T. Yatagai, W. Jiang, A. Endo, P. Dunne, and G. O'Sullivan, Appl. Phys. Lett. **97**, 111503 (2010).

[31] D. Kilbane and G. O'Sullivan, J. Appl. Phys. **108**, 104905 (2010).

[32] R. D. Cowan, *The Theory of Atomic Structure and Spectra* (University of California Press, Berkeley, CA, 1981).

[33] S. S. Churilov, R. R. Kilidiyarova, A. N. Ryabtsev, and S. V. Sadovsky, Phys. Scr. **80**, 045303 (2009).

[34] G. O'Sullivan, P. K. Carroll, P. Dunne, R. Faulkner, C. McGuinness, and N. Murphy, J. Phys. B **32**, 1893 (1999).

[35] G. O'Sullivan, J. Phys. B **16**, 3291 (1983).

[36] C. F. Fischer, Comput. Phys. Commun. **4**, 107 (1972).

[37] M. F. Gu, Astrophys. J. **582**, 1241 (2003).